EPJ Web of Conferences **40**, 08004 (2013)
DOI: 10.1051/epjconf/20134008004

Structure analysis of Ni thin films epitaxially grown on bcc metal underlayers formed on MgO(100) substrates

Mitsuru Ohtake, Takato Yanagawa, Jumpei Higuchi, and Masaaki Futamoto

Faculty of Science and Engineering, Chuo University, 1-13-27 Kasuga, Bunkyo-ku, Tokyo 112-8551, Japan

Abstract. Ni thin films are prepared on Cr, V, and Nb underlayers with bcc structure formed on MgO(100) single-crystal substrates by molecular beam epitaxy. The growth behavior and the crystallographic properties are investigated by *in-situ* reflection high-energy electron diffraction and pole-figure X-ray diffraction. Cr(100) and V(100) single-crystal underlayers grow epitaxially on the substrates, whereas an Nb epitaxial underlayer consisting of two bcc(110) variants is formed on the MgO(100) substrate. Metastable hcp-Ni(11$\bar{2}$0) crystals nucleate on the Cr and the V underlayers, where the metastable hcp structure is stabilized through hetero-epitaxial growth. With increasing the film thickness, the hcp structure starts to transform into more stable fcc structure by atomic displacement parallel to the hcp(0001) close-packed plane. The resulting films are consisting of mixtures of hcp and fcc crystals. On the other hand, only the formation of fcc crystal is recognized for the Ni film grown on Nb(110) underlayer.

1 Introduction

Applications of 3*d* ferromagnetic transition metal thin films with metastable crystallographic structures are recently expected to yield new possibilities in the development of magnetic devices. For example, tri-layer films consisting of MgO and metastable bcc-Co layers are reported to show high tunnelling magnetoresistance ratios [1, 2]. In order to apply the films for practical applications, it is necessary to understand the formation conditions of metastable magnetic films.

Epitaxial thin film growth has been investigated for 3*d* ferromagnetic transition metals by employing various single-crystal substrates or underlayers [3]–[6], and it has been shown that magnetic thin films with metastable crystal structures can be prepared [7, 8]. Ni is a typical soft magnetic material and its crystal structure is fcc up to the melting point in the bulk phase diagram. Ni epitaxial films with metastable bcc structure have been formed on GaAs substrates [9]–[11], whereas metastable hcp-Ni epitaxial films have been prepared on MgO [12, 13], Au [14, 15], Cr [16], and Ru [17] materials. However, these metastable crystals transformed into more stable fcc structure during film preparation processes and these films generally include a large volume of fcc phase. In our previous studies, formations of Ni epitaxial films with metastable bcc [10, 11] and hcp [15]–[17] structures were investigated and their transformation processes from metastable structures to more stable fcc structure were discussed.

Epitaxial thin film growth is delicately influenced by the formation conditions like the underlayer material, the underlayer orientation, etc. bcc metal underlayers such as Cr and V have been frequently used to prepare hcp-Co thin films with the *c*-axis parallel to the substrate surface [18, 19]. bcc metals are expected to also stabilize the hcp structure for Ni film. In the present study, Ni thin films are prepared on Cr, V, and Nb underlayers formed on MgO(100) single-crystal substrates. The growth behavior and the crystallographic properties are investigated.

2 Experimental procedure

Thin films were prepared on polished MgO(100) substrates by using a molecular beam epitaxy system equipped with facilities of arc plasma sputtering (ARL-300, ULVAC Inc.) and electron-beam evaporation sources. The base pressures were lower than 3×10^{-8} Pa. Before film formation, substrates were heated at 500 °C for 1 h to obtain clean surfaces. The surface structure was checked by reflection high-energy electron diffraction (RHEED). Figure 1(a-1) shows the RHEED pattern observed for an MgO(100) substrate after heating. The pattern corresponds to a clean MgO substrate, as shown in the schematic diagram of figure 1(a-2). 10-nm-thick Cr, V, and Nb underlayers were deposited on substrates at 300 °C by arc plasma sputtering. The substrate temperature was used to promote epitaxial growth of bcc underlayers on MgO(100) substrates. The arc voltage was fixed at 100 V. 40-nm-thick Ni films were deposited on the bcc underlayers at room temperature by electron-beam evaporation.

The surface structure during film formation was observed by *in-situ* RHEED. The crystallographic properties were investigated by $2\theta/\omega$-scan (out-of-plane)

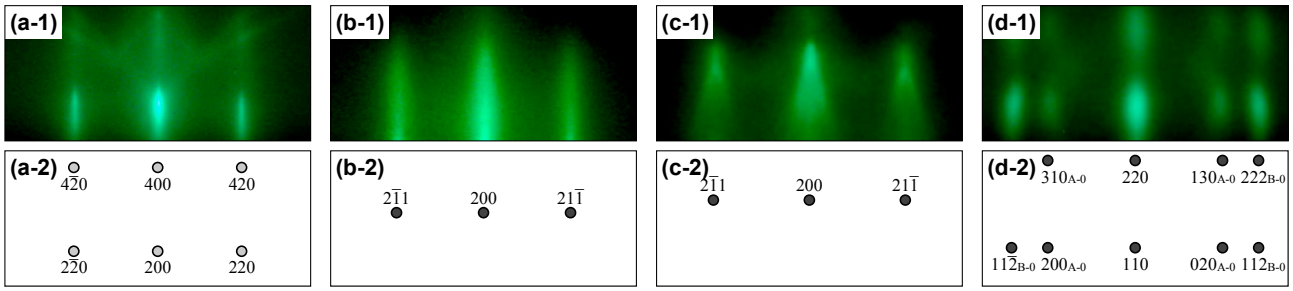

Fig. 1. (a-1)–(d-1) RHEED patterns and (a-2)–(d-2) the schematic diagrams of an MgO(100) substrate and (b) Cr, (c) V, and (d) Nb underlayers formed on MgO substrates. The incident electron beam is parallel to MgO[001].

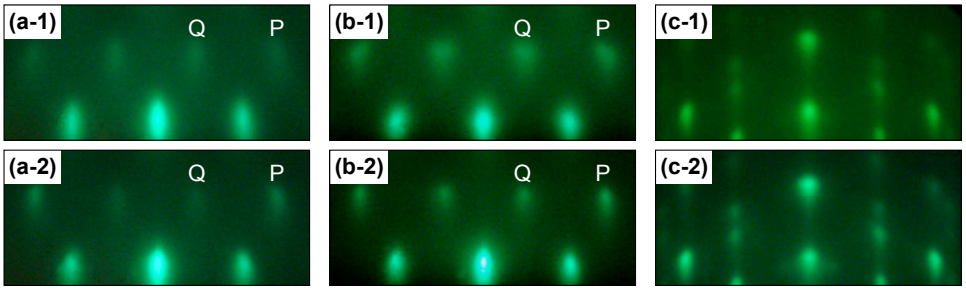

Fig. 2. RHEED patterns observed for Ni thin films grown on (a) Cr, (b) V, and (c) Nb underlayers hetero-epitaxially grown on MgO(100) substrates. The film thicknesses are (a-1)–(c-1) 2 and (a-2)–(c-2) 40 nm. The incident electron beam is parallel to MgO[001].

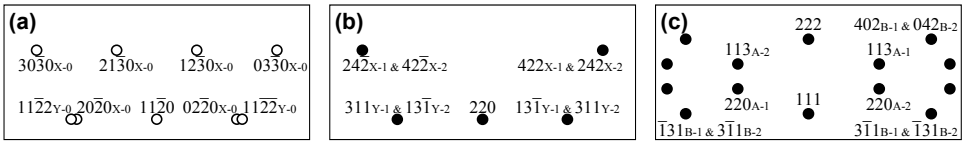

Fig. 3. Schematic diagrams of RHEED patterns simulated for (a) hcp(11$\bar{2}$0), (b) fcc(110), and (c) fcc(111) surfaces. The diagrams are calculated by using lattice constants of $a_{\text{fcc-Ni}} = 0.352$ nm, $a_{\text{hcp-Ni}} = 0.249$ nm, and $c_{\text{hcp-Ni}} = 0.415$ nm [16]. The incident electron beam is parallel to (a) $[0001]_{\text{X-0}}$ and $[1\bar{1}00]_{\text{Y-0}}$, (b) $[1\bar{1}\bar{1}]_{\text{X-1}}$, $[1\bar{1}1]_{\text{X-2}}$, $[\bar{1}1\bar{2}]_{\text{Y-1}}$, and $[1\bar{1}\bar{2}]_{\text{Y-2}}$, or (c) $[1\bar{1}0]_{\text{A-1}}$, $[\bar{1}10]_{\text{A-2}}$, $[11\bar{2}]_{\text{B-1}}$, and $[\bar{1}\bar{1}2]_{\text{B-2}}$.

and pole-figure X-ray diffraction (XRD) with Cu-Kα radiation ($\lambda = 0.15418$ nm).

3 Results and discussion

Figures 1(b-1) and (c-1) show the RHEED patterns of Cr and V underlayers observed after deposition on MgO(100) substrates, respectively. Clear diffraction patterns corresponding to bcc(100) single-crystal surfaces are observed, as shown in the schematic diagrams of figures 1(b-2) and (c-2). The epitaxial orientation relationships are determined by RHEED as

$$\text{Cr}(100)[011]_{\text{bcc}} \parallel \text{MgO}(100)[001],$$
$$\text{V}(100)[011]_{\text{bcc}} \parallel \text{MgO}(100)[001].$$

Cr and V single-crystal underlayers of (100) orientation are formed. Figure 1(d-1) shows the RHEED pattern of an Nb underlayer observed after deposition. A clear diffraction pattern corresponding to bcc(110) texture is recognized. The pattern consists of two bcc(110) reflections, as shown by the spots, A-0 and B-0, in the spot schematic diagram of figure 1(d-2). The epitaxial orientation relationships of

$$\text{Nb}(110)[001]_{\text{bcc}} \parallel \text{MgO}(100)[001] \quad \text{(type A-0)},$$
$$\text{Nb}(110)[1\bar{1}0]_{\text{bcc}} \parallel \text{MgO}(100)[001] \quad \text{(type B-0)}$$

are determined. An Nb epitaxial underlayer consisting of two bcc(110) variants, whose orientations are rotated around the film normal by 90° each other, is formed.

Figures 2(a-1)–(a-2) and 2(b-1)–(b-2) show the RHEED patterns observed during Ni depositions on the Cr(100) and the V(100) underlayers, respectively. In the early stages of film growth on both underlayers [figures 2(a-1, b-1)], clear diffraction patterns corresponding to hcp(11 $\bar{2}$ 0) texture are observed, as shown in the schematic diagram of figure 3(a). Metastable hcp-Ni epitaxial films are obtained on the Cr(100) and the V(100) underlayers. The RHEED pattern is analyzed to be an overlap of two hcp(11$\bar{2}$0) reflections, as shown by the spots, X-0 and Y-0, in the schematic diagram of figure 3(a). The epitaxial orientation relationships are determined by RHEED as

$$\text{Ni}(11\bar{2}0)[0001]_{\text{hcp}} \parallel \text{Cr, V}(100)[011] \quad \text{(type X-0)},$$
$$\text{Ni}(11\bar{2}0)[1\bar{1}00]_{\text{hcp}} \parallel \text{Cr, V}(100)[011] \quad \text{(type Y-0)}.$$

The hcp-Ni films consist of two (11$\bar{2}$0) variants, whose *c*-axes are in-plane and rotated around the film normal by 90° each other. The epitaxial orientation relationships are similar to the case of hcp-Co films epitaxially grown on bcc(100) underlayers [18].

As the film thickness increases [figures 2(a-2, b-2)], reflection intensities of 11$\bar{2}$0, $20\bar{2}0_{\text{X-0}}$, $02\bar{2}0_{\text{X-0}}$, $03\bar{3}0_{\text{X-0}}$, $2\bar{1}\bar{1}0_{\text{Y-0}}$, and $\bar{1}2\bar{1}0_{\text{Y-0}}$ RHEED spots increase, whereas those of $21\bar{3}0_{\text{X-0}}$ and $12\bar{3}0_{\text{X-0}}$ spots decrease. This result suggests that other reflections are overlapping with the hcp(11$\bar{2}$0) reflections. The reflections overlapped with the hcp reflections are determined to be four fcc(110) reflections, as shown by the spots, X-1, X-2, Y-1, and

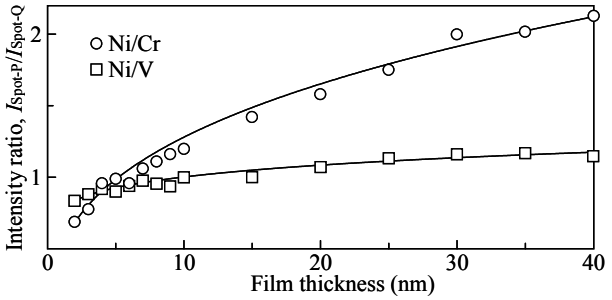

Fig. 4. Dependence of film thickness on the RHEED reflection intensity ratio of $03\bar{3}0_{X\text{-}0}$ spot (spot-P) to $12\bar{3}0_{X\text{-}0}$ spot (spot-Q).

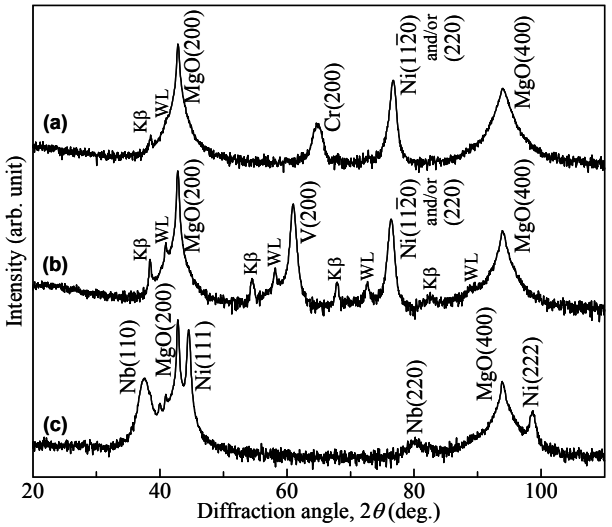

Fig. 5. Out-of-plane XRD spectra of Ni films grown on (a) Cr, (b) V, and (c) Nb underlayers formed on MgO(100) substrates. The intensity is shown in a logarithmic scale.

Y-2, in the schematic diagram of figure 3(b). The crystallographic orientation relationships between the hcp and the fcc crystals are determined as

$$\text{fcc}(110)[1\bar{1}\bar{1}] \parallel \text{hcp}(11\bar{2}0)[0001]_{X\text{-}0} \quad \text{(type X-1)},$$
$$\text{fcc}(110)[1\bar{1}1] \parallel \text{hcp}(11\bar{2}0)[0001]_{X\text{-}0} \quad \text{(type X-2)},$$
$$\text{fcc}(110)[\bar{1}1\bar{2}] \parallel \text{hcp}(11\bar{2}0)[1\bar{1}00]_{Y\text{-}0} \quad \text{(type Y-1)},$$
$$\text{fcc}(110)[1\bar{1}2] \parallel \text{hcp}(11\bar{2}0)[1\bar{1}00]_{Y\text{-}0} \quad \text{(type Y-2)}.$$

These crystallographic relationships are similar to the Shoji-Nishiyama orientation relationship [20, 21]. In these configurations, the close-packed planes of hcp crystal are parallel to those of fcc crystal. The hcp structure in the Ni film is apparently transforming into more stable fcc structure through atomic displacement parallel to the hcp(0001) close-packed plane. The transformation behavior is similar to the cases of hcp-Ni(11$\bar{2}$0)/Au(100) [15] and hcp-Ni(1$\bar{1}$00)/Cr(211) [16] systems, though the underlayer is different.

Figure 4 shows the film thickness dependence on the reflection intensity ratio of $03\bar{3}0_{X\text{-}0}$ spot (spot-P) to $12\bar{3}0_{X\text{-}0}$ spot (spot-Q), $I_{spot\text{-}P}/I_{spot\text{-}Q}$. For both cases, Ni film growth either on Cu or V underlayer, the ratio gradually increases with increasing the film thickness. The increase in intensity ratio shows that the ratio of fcc to hcp crystal exposed to the film surface increases with increasing the film thickness. It is also shown that the thickness dependence differs between the two cases. The hcp structure is more stable in the Ni film formed on V underlayer than in the Ni film formed on Cr underlayer.

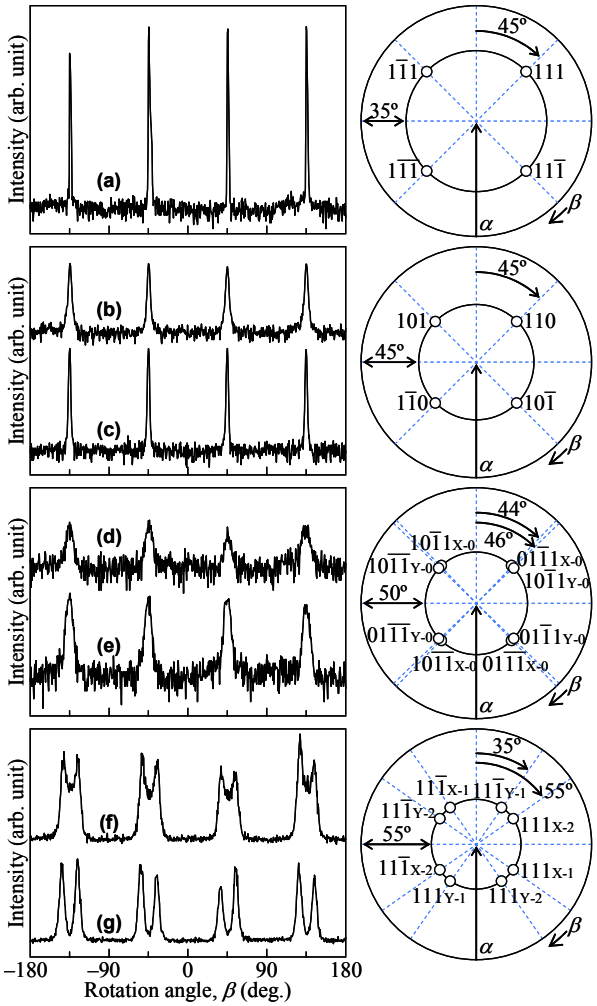

Fig. 6. Pole-figure XRD spectra of (a) an MgO(100) substrate, (b) Cr(100) and (c) V(100) underlayers formed on MgO substrates, (d, e) hcp(11$\bar{2}$0) crystals in Ni films formed on (d) Cr and (e) V underlayers, and (f, g) fcc(110) crystals in Ni films formed on (f) Cr and (g) V underlayers. The spectra are measured by fixing the angles of (α, 2θB) at (a) (35°, 37°), (b) (45°, 44°), (c) (45°, 42°), (d, e) (50°, 48°), or (f, g) (55°, 45°).

The resulting film structure was investigated by out-of-plane and pole-figure XRD analyses. Figures 5(a) and (b) show the out-of-plane XRD spectra of Ni films grown on Cr(100) and V(100) underlayers, respectively. Clear reflections corresponding to hcp-Ni(11$\bar{2}$0) and/or fcc-Ni(220) are observed around the diffraction angle, 2θ, of 76° in addition to MgO(200) and Cr(200) or V(200) reflections.

Figure 6(a) shows the pole-figure XRD spectrum of MgO(100) substrate measured by fixing the tilt and the diffraction angels of (α, 2θB) at (35°, 37°), where MgO{111} reflections are expected to be detectable. Four-fold symmetry reflections are clearly observed. Figures 6(b) and (c), respectively, show the pole-figure spectra of Cr(100) and V(100) underlayers measured by fixing the angles of (α, 2θB) at (45°, 44°) and (45°, 42°), where bcc{110} reflections from underlayers are expected to be observed. Four reflections are observed in both the spectra. Figures 6(d) and (e), respectively, show the pole-figure spectra of hcp(11$\bar{2}$0) crystals in Ni films formed on Cr and V underlayers measured by fixing the (α, 2θB) at (50°, 48°), where hcp{1$\bar{1}$01} reflections are

expected to be observed. Four reflections which originate from two hcp(11$\bar{2}$0) variants with two-fold symmetry with respect to perpendicular direction are recognized. The reflection intensity of hcp crystal in Ni film formed on V underlayer is stronger than that of hcp crystal in Ni film formed on Cr underlayer. The result also shows that the hcp structure is more stable on V underlayer than on Cr underlayer. Figures 6(f) and (g) show the spectra of fcc(110) crystals measured by fixing the (α, $2\theta B$) at (55°, 45°), where fcc{111} reflections are expected to appear. Eight reflections which originate from four fcc(110) variants with two-fold symmetry with respect to perpendicular direction are recognized. By considering the relationships of α and β (rotating angle) for these reflections, the epitaxial and the transformation orientation relationships determined by RHEED are confirmed.

Figure 2(c) shows the RHEED patterns observed for an Ni film formed on Nb(110) underlayer. A clear diffraction pattern corresponding to fcc(111) texture starts to be observed from the beginning of Ni deposition and it remains unchanged during 40-nm-thick Ni film formation. The fcc(111) pattern is analyzed to be an overlap of four reflections, as shown by the spots, A-1, A-2, B-1, and B-2, in the schematic diagram of figure 3(c). The epitaxial orientation relationships are determined by RHEED as

$$\mathrm{Ni}(111)[1\bar{1}0]_{\mathrm{fcc}} \parallel \mathrm{Nb}(110)[001]_{\mathrm{A\text{-}0}} \text{ (type A-1)},$$

$$\mathrm{Ni}(111)[1\bar{1}0]_{\mathrm{fcc}} \parallel \mathrm{Nb}(110)[001]_{\mathrm{A\text{-}0}} \text{ (type A-2)},$$

$$\mathrm{Ni}(111)[11\bar{2}]_{\mathrm{fcc}} \parallel \mathrm{Nb}(110)[1\bar{1}0]_{\mathrm{B\text{-}0}} \text{ (type B-1)},$$

$$\mathrm{Ni}(111)[\bar{1}\bar{1}2]_{\mathrm{fcc}} \parallel \mathrm{Nb}(110)[1\bar{1}0]_{\mathrm{B\text{-}0}} \text{ (type B-2)}.$$

An Ni epitaxial film consisting of four fcc(111) variants is formed. The atomic stacking sequence of close-packed plane along the perpendicular direction is different between fcc crystals with types of A-1 and A-2 or B-1 and B-2. Figure 5(c) shows the out-of-plane XRD spectrum of Ni film grown on Nb underlayer. bcc-Nb(110) and fcc-Ni(111) reflections are recognized in addition to MgO(200) reflection.

The reason why such fcc(111) crystal growth is observed on Nb(110) underlayer may be explained by considering the nature of close-packed plane. As shown previously for the cases of metastable hcp-Ni(11$\bar{2}$0) crystals formed on Cr and V underlayers, the metastable hcp structure transforms into fcc structure through atomic displacement parallel to the close-packed plane. The first Ni atomic layer deposited on Nb(110) underlayer is strongly influenced by the Nb underlayer. The second and the third Ni atomic layers are less influenced than the first Ni layer. In this case, the Ni film will more favorably take fcc crystal structure, since the close-packed plane of Ni film is parallel to the underlayer surface. Thus, the Ni film on Nb(110) underlayer is considered to grow with more stable fcc structure from an early stage of film growth.

4 Conclusions

The growth behavior and the crystallographic properties of Ni films formed on Cr, V, and Nb underlayers with bcc structure hetero-epitaxially grown on MgO(100) substrates are investigated by RHEED and XRD. bcc-Cr and bcc-V single-crystal underlayers of (100) orientation are obtained, while a bcc-Nb epitaxial underlayer consisting of bcc(110) variants is formed on MgO(100) substrate. Metastable hcp-Ni(11$\bar{2}$0) crystals epitaxially nucleate on the Cr and the V underlayers, where the hcp structure is stabilized through hetero-epitaxial growth. As the thickness increases, the hcp structure starts to transform into more stable fcc structure by atomic displacement parallel to the hcp(0001) close-packed plane. On Nb(110) underlayer, only the stable fcc-Ni crystal growth with (111) orientation is recognized.

Acknowledgements

A part of this work was supported by MEXT-Japan and Hattori-Hokokai.

References

1. X. -G. Zhang, W. H. Butler, Phys. Rev. B **70**, 172407 (2004)
2. S. Yuasa, A. Fukushima, H. Kubota, Y. Suzuki, K. Ando, Appl. Phys. Lett. **89**, 042505 (2006)
3. E. F. Wassermann, H. P. Jablonski, Surf. Sci. **22**, 69 (1970)
4. G. A. Prinz, J. J. Krebs, Appl. Phys. Lett. **39**, 397 (1981)
5. M. Thompson, J. L. Erskine, Phys. Rev. B **31**, 6832 (1985)
6. B. Voigtländer, G. Meyer, N. M. Amer, Phys. Rev. B **44**, 10354 (1991)
7. M. Onellion, C. L. Fu, M. A. Thompson, J. L. Erskine, A. J. Freeman, Phys. Rev. B **33**, 7322 (1986)
8. G. A. Prinz, Phys. Rev. Lett. **54**, 1051 (1985)
9. C. S. Tian, D. Qian, D. Wu, R. H. He, Y. Z. Wu, W. X. Tang, L. F. Yin, Y. S. Shi, G. S. Dong, X. F. Jin X. M. Jiang, F. Q. Liu, H. J. Qian, K. Sun, L. M. Wang, G. Rossi, Z. Q. Qiu, J. Shi, Phys. Rev. Lett. **94**, 137210 (2005)
10. M. Ohtake, Y. Nonaka, M. Futamoto, IEEE Trans. Magn. **48**, 1589 (2012)
11. M. Ohtake, M. Futamoto, N. Inaba, JEMS 2012.
12. W. Tian, H. P. Sun, X. Q. Pan, J. H. Yu, M. Yeadon, C. B. Boothroyd, Y. P. Feng, R. A. Lukaszew, R. Clarke, Appl. Phys. Lett. **86**, 131915 (2005)
13. T. Tanaka, T. Nishiyama, K. Shikada, M. Ohtake, F. Kirino, M. Futamoto, J. Magn. Soc. Jpn. **34**, 21 (2010)
14. P. Bayle-Guillemaud, J. Thibault, Philos. Mag. A **77**, 475 (1998)
15. M. Ohtake, Y. Sato, J. Higuchi, T. Tanaka, F. Kirino, M. Futamoto, Jpn. J. Appl. Phys. **50**, 103001 (2011)
16. M. Ohtake, Y. Sato, J. Higuchi, M. Futamoto, J. Phys.: Conf. Ser. **266**, 012122 (2011)
17. J. Higuchi, M. Ohtake, Y. Sato, T. Nishiyama, M. Futamoto, Jpn. J. Appl. Phys. **50**, 063001 (2011)
18. A. Nakamura, M. Futamoto, Jpn. J. Appl. Phys. **32**, L1410 (1993)
19. C. K. Lo, I. Klik, C. P. Chang, Y. Liou, C. S. Yang, Y. D. Yao, J. A. C. Huang, Appl. Sur. Sci. **113–114**, 160 (1997)
20. H. Shoji, Z. Kristallogr. **84**, 74 (1932)
21. Z. Nishiyama, Sci. Rep. Res. Inst. Tohoku Univ. A **25**, 76 (1936)